ACCSCIENCE PUBLISHING

International Journal of Bioprinting

RESEARCH ARTICLE

3D-printed devices for optimized generation of cold atmospheric plasma to improve decontamination of surfaces from respiratory pathogens

Asma Bouazizi[1,2†], Klára Obrová[1†], Eva Vaňková[3,4†], Anna Machková[3], Josef Khun[3], Romana Hadravová[5], Jan Hodek[5], Lucie Ulrychová[5,6], Abdelhalim Trabelsi[2], Jan Weber[5], Leonardo Zampieri[7], Fabio Avino[8], Ivo Furno[8], Vladimír Scholtz[3*], and Thomas Lion[1,9*]

[1] St. Anna Children's Cancer Research Institute (CCRI), Vienna, Austria

[2] Research Laboratory of Epidemiology and Immunogenetics of Viral Infections (LR14SP02), Faculty of Pharmacy, University of Monastir, Tunisia

[3] Department of Physics and Measurements, University of Chemistry and Technology, Prague, Czech Republic

[4] Department of Biotechnology, University of Chemistry and Technology, Prague, Czech Republic

[5] Institute of Organic Chemistry and Biochemistry of the Czech Academy of Sciences, Prague, Czech Republic

[6] Department of Genetics and Microbiology, Charles University, Faculty of Sciences, Czech Republic

[7] Department of Physics, University of Milano Bicocca, Milano, Italy

[8] Ecole Polytechnique Fédérale de Lausanne (EPFL), Swiss Plasma Center (SPC), Lausanne, Switzerland

[9] Department of Pediatrics, Medical University of Vienna, Vienna, Austria

[†] These authors contributed equally to this work.

***Corresponding authors:**
Thomas Lion (thomas.lion@ccri.at)

Vladimír Scholz (Vladimir.Scholtz@vscht.cz)

Citation: Bouazizi A, Obrová K, Vaňková E, et al. 3D-printed devices for optimized generation of cold atmospheric plasma to improve decontamination of surfaces from respiratory pathogens. *Int J Bioprint*. 2024. doi: 10.36922/ijb.3679

Received: May 16, 2024
Accepted: July 11, 2024
Published Online: August 28, 2024

Abstract

Three-dimensional (3D)-printing technology is instrumental in creating devices for biological applications, including the exploitation of cold atmospheric plasma (CAP). CAP, a partially ionized gas that functions at ambient temperatures, serves as a safe, inexpensive, and effective tool for the inactivation of various pathogens on different surfaces. In this study, we compared three different 3D-printed devices with respect to their ability to provide optimized CAP compositions effective against select respiratory viruses (SARS-CoV-2, influenza virus, adenovirus, and rhinovirus) and the bacterium *Pseudomonas aeruginosa*, which is associated with serious lung diseases. The transmission of respiratory pathogens via surface contamination may pose a serious health threat, thus highlighting the biological importance of the current study. The properties of a prototype 3D-printed CAP-generating device and two optimized versions were characterized by detecting reactive oxygen and nitrogen species (RONS) in a gaseous environment via infrared spectroscopy and analyzing the composition of the reactive compounds. The virucidal effects of CAP were examined by determining virus infectivity and particle integrity. The bactericidal effect was documented by viability testing and visualization via transmission electron microscopy. The findings indicate that optimization of the 3D-printed devices for CAP production yielded an environment with relatively high amounts of RONS (O_3, N_2O,

NO_2, and H_2O_2), reducing the exposure time required for inactivation of respiratory pathogens by approximately 50%. In addition to reducing infectivity and viability, CAP treatment led to the destruction of viral nucleic acids and physical damage to bacterial cells. Owing to its flexibility and easy implementation, optimized CAP generated by 3D-printed devices provides an attractive inactivation method adaptable for different biological applications, including surface decontamination from viral and bacterial pathogens.

Keywords: 3D-printed devices; Adenovirus; Disinfection; Influenza A; *Pseudomonas aeruginosa*; Reactive oxygen species; Rhinovirus; SARS-CoV-2

1. Introduction

Three-dimensional (3D)-printing technology is a powerful and readily implementable approach for creating devices for diverse biological applications. The moldability provided by 3D printing technology, with its highly flexible design of external and internal structures, allows for the optimization of the physical properties of cold atmospheric plasma (CAP) or nonthermal plasma (NTP). These properties are significantly influenced by the geometry of 3D-printed devices. The biological exploitation of CAP is an emerging technology for decontaminating various types of liquids, medical materials, devices, and even surfaces across diverse industries. Additionally, the antimicrobial effects of CAP are well documented.[1–7] Compared with conventional decontamination techniques, CAP has several advantages, such as on-demand operation (easy on/off switching), simple handling, low cost and maintenance, performance at ambient temperature and atmospheric pressure, and the ability to function in dry conditions. CAP has been applied in a wide range of fields, including physics, chemistry, biological sciences, life sciences, and medicine.[8–14]

Biomaterial-associated microbial contamination in biologically conducive 3D tissue-engineered constructs has greatly limited the clinical application of scaffold systems.[15,16] Although antimicrobial biomaterials are being developed to prevent such infections,[17,18] their use in bioprinting-based approaches for scaffold fabrication has not been thoroughly examined to date. Therefore, CAP may emerge as an alternative technical approach for surface decontamination of bioprinted materials in the future. The bactericidal effects of CAP are well established, but research on its effectiveness against pathogenic viruses remains relatively limited,[19–24] despite several reviews that have been published.[25–27] The virucidal mechanism of CAP is influenced by the characteristics of the plasma-generating devices, specifically their geometry, electric voltage and current applied, and several other application parameters.[28] CAP is produced by ionizing a neutral gas, e.g., ambient air, using a source of energy such as electric discharge.[29] The ionized gas is composed of reactive oxygen and nitrogen species (RONS; e.g., OH, H_2O_2, NO, and NO_2), radicals, free electrons, electric fields, heat, and other elements.[12] In propagating ionization waves, the gas draws particles out of the electrode area, forming a stream of (re)active particles that fills the entire reaction chamber (Figure 1).[29] Microbial inhibition by CAP is hypothesized to result from several processes. Some researchers discovered that active plasma particles target proteins, DNA, the cell wall, and membranes. For example, oxygen species, such as O (singlet oxygen) and O_3 (ozone), may physically affect the cell membrane and cause DNA damage.[30] O_3 has been reported as the main[24] or additional factor[31,32] involved in the inactivation of the bacteriophage MS2[33] and human adenovirus (HAdV).[34] Hydrogen peroxide (H_2O_2) has been suggested to be crucial for the inactivation of respiratory syncytial virus (RSV)[35] and influenza A virus (IAV)[36] but to play only a minor role in the inactivation of HAdV.[37] RONS can damage cells by reacting with various cellular biomacromolecules, such as proteins, lipids, and DNA.[38] As CAP components can enter cells, it is not surprising that cell organelles, such as mitochondria and nuclei, are affected.[39] Additionally, direct damage to nucleic acids and proteins has been reported.[40] These findings contribute to the reported effective disinfection of various microorganisms.[19] Pathogens can undergo oxidative damage from various RONS,[41] and the synergistic effect of combining these reactive species in CAP can increase their efficiency. A significant challenge lies in the precise control of CAP parameters. Surface decontamination may be more effective when physical parameters are optimized to produce specific concentrations of individual RONS.

Human respiratory pathogens, including viruses (e.g., severe acute respiratory syndrome coronavirus 2 [SARS-CoV-2], IAV, HAdV, and human rhinovirus [HRV]) and bacteria (e.g., *Pseudomonas aeruginosa*), can spread via different modes of transmission, and the control of contaminated surfaces is an important measure in different settings.[42–46] Human coronaviruses, such as SARS-CoV-2, frequently emerge globally because of their rapid evolution characterized by high rates of nucleotide substitution and recombination, as documented by the

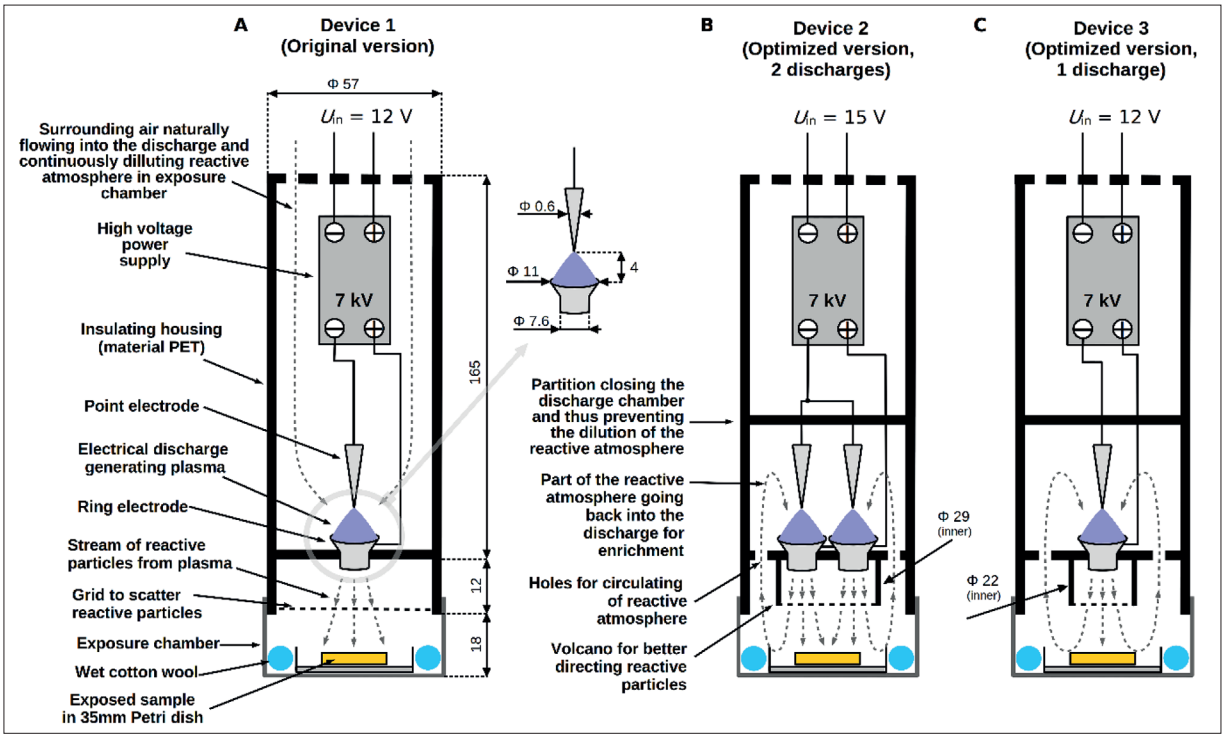

Figure 1. Schematic representation of 3D-printed cold atmospheric plasma (CAP)-generating devices: (A) Device 1: Original version with an opening for fresh air supply and ventilation; (B) Device 2: Optimized version enclosed in a chamber with a double discharge; (C) Device 3: Optimized version enclosed in a chamber with a single discharge. Abbreviations: PET: polyethylene terephthalate; U_{in}: input voltage; Φ: diameter.

recent pandemic.[47] IAV infects a variety of species and mutates frequently, resulting in antigenic drift and shift. These processes contribute to repeated seasonal outbreaks and epidemics.[48] HAdV and HRV are highly contagious pathogens linked to a variety of respiratory diseases.[49,50] Although respiratory diseases caused by HAdV and HRV typically have moderate effects, they can cause substantial morbidity and economic impacts. *P. aeruginosa* is a frequently observed opportunistic pathogen that mainly infects the respiratory tract, with potentially severe disease, particularly in immunocompromised patients.[51,52] Owing to the potential role of fomites, such as doorknobs, utensils, and other commonly touched surfaces, in the transmission of these pathogens, the development of efficient surface disinfection strategies is crucial for infection control.

In the present study, we aimed to optimize the CAP technology generated by 3D-printed devices for the biological inactivation of respiratory pathogens. These were represented by four viruses with diverse features (SARS-CoV-2, IAV, HAdV, and HRV) and a clinically challenging bacterium (*P. aeruginosa*). The selected model microorganisms were included to encompass significant and widely encountered pathogens, each displaying distinct biological features that could affect the efficiency of decontamination. Our 3D-printed CAP devices are based on direct current (DC) corona discharge, which uses HV sources with low current outputs that are inherently safe (i.e., no risk of electric shock), and the devices are very cheap. Two optimized 3D-printed portable CAP-generating devices were also created, and their performance was compared to that of the original version used in previous investigations (Figure 1).[19] The detection of RONS produced by individual devices displayed obvious differences, which translated into enhanced virucidal and bactericidal effects. Unlike previous studies, we used a panel of human respiratory pathogens with epidemic potential and comprehensively investigated CAP efficiency, linking enhanced production of RONS species to improved efficiency. The flexibility and easy application of CAP decontamination via 3D-printed devices highlights the significant potential of this technology for pathogen inactivation, and the presented data pave the way for its further development and implementation in various applications.

2. Methods

2.1. CAP devices

Cold atmospheric plasma (CAP) was generated by corona discharges in three different 3D-printed devices (hereinafter referred to as devices 1, 2, and 3; Figure 1). The external appearance of the devices is displayed in Figure S1 (Supplementary File). The device bodies were fabricated via a Prusa i3 MK3 3D printer (Prusa Research, Czech Republic) from polyethylene terephthalate glycol-modified (PETG), which was selected for its superior chemical resistance, mechanical strength, and thermal stability. These properties ensure structural integrity under the thermal stresses encountered during plasma operations (Table 1).

These settings were meticulously selected to optimize the manufacturing process and enhance the functionality and durability of the CAP devices. Precise control of 3D -printing parameters, such as the nozzle temperature and print speed, plays a critical role in achieving the high-quality builds required for reliable plasma generation.

Devices with specific dimensions were developed to ensure plasma discharge and stability. The selection of PETG as the material was crucial because of its mechanical properties, ease of printing, and minimal warping tendencies, which are essential for maintaining the accuracy of the printed components. Furthermore, a 20% infill density was selected to provide a balance between structural integrity and material efficiency, ensuring that the devices remain lightweight yet strong enough to withstand operational stresses.

The devices are robust and impact resistant and are thus appropriate for daily use in a variety of settings. The minimum force capable of damaging the functional properties of the device was assessed and demonstrated to require dropping the device from at least 1 m onto a hard surface. The device resisted a breaking force of up to 500 N on the 3D-printed package and a continuous force of 100 N on the mesh, protecting the electrode hole. At 150 N, the mesh was deformed but not destroyed.

Table 1. Material specifications for 3D printing

Property	Specification
Printer model	Prusa i3 MK3
Material	Polyethylene terephthalate glycol-modified (PETG)
Layer resolution (mm)	0.05
Nozzle temperature (°C)	240–250
Bed temperature (°C)	75–85
Infill density (%)	20 (for a balance of lightness and durability)
Head printing speed (mm/s)	60 (optimized for precision)
Shell thickness	
Perimeter (mm)	0.4
Top/bottom (mm)	0.2
Filament flow (%)	95
Infill pattern	Linear grid (tilted by 45°)

2.1.1. Device 1

Device 1, referred to as the original device, was studied in our previous work[19] and served as a benchmark in the current study. CAP is generated by negative DC point-to-ring corona discharge, where the point electrode is a syringe needle (MEDOJECT 0.6 × 25 mm intramuscular injection needle; CHIRANA T. Injecta, Czech Republic) and the conical-shaped ring electrode consists of brass. The top of the ring electrode (~11 mm in diameter) is placed 3.3 mm below the tip of the needle and connected to the positive terminal of an HV source, whereas the needle electrode is connected to the negative terminal. The negative corona discharge is formed in the vicinity of the tip, whereas the positive corona discharge burns at the edge of the ring. This creates a bipolar corona discharge, where reactive species are carried with ions accelerated in the electric field between the electrodes. The discharge current was set at 150 μA, and the voltage was set at 7 kV, resulting in a power of 1.05 W, which was achieved through precise positioning of the tip of the needle relative to the ring. The discharge burns in pulse-less mode, as previously described.[53] The ion wind produced by the discharge draws air through the upper holes and directs it toward the sample. Cotton wool wetted with 10 mL of water was placed around the sample to increase the humidity, which reached over 90% in all the samples. Further details and dimensions are displayed in Figure 1A. To optimize the virucidal and microbicidal efficiency, two additional devices (devices 2 and 3) were developed.

2.1.2. Device 2

Device 2 is developed with the same type of discharge as device 1 but with two discharges. The discharge current and voltage were set identically to those of device 1 at 100 μA and 7 kV, respectively, resulting in a power of 1.4 W. The internal geometric arrangement was modified to prevent fresh air ventilation. The ions circulate from the discharge point toward the sample and back to the point electrode through the holes around the ring electrode. In addition, to improve the direction of the active particle stream from the discharge plasma to the exposed sample, a "volcano" design was incorporated into this device. The design features a tube with an internal diameter of 30 mm and a height of 10 mm attached to the outlet of the ring electrode. A fine metallic mesh (mesh size: 0.5 × 0.5 mm; wire thickness: 0.2 mm) is placed at the end of the "volcano" to ensure safety by preventing electrode contact and mediating a more homogeneous distribution of active

particles within the chamber space. Further details on the arrangement and dimensions are displayed in Figure 1B.

2.1.3. Device 3

Device 3 has the same type of discharge as devices 1 and 3 but with a single discharge copy (power: 0.7 W). The internal arrangement is identical to that of device 2, except for the inner diameter of the "volcano," which surrounds only one discharge and thus has a smaller diameter of 22 mm. Further details on the arrangement and dimensions are displayed in Figure 1C.

2.2. Characterization of RONS

The production of RONS, which are known virucidal and microbicidal agents, can be monitored by detecting the long-lived final products NO, NO_2, and O_3. It is assumed that their concentrations are proportional to the concentrations of short-lived reactive particles.

The concentrations of NO and NO_2 were measured via chemiluminescence detection via a Serinus 40H NO_x analyzer (range: up to 1000 ppm; accuracy: 2%; ACOEM Ecotech, UK). Gas from the active region of the devices was led to the analyzer through a 1 m-long polytetrafluoroethylene (PTFE) tube with an inner diameter of 3 mm, and the measured values were recorded.

The concentrations of O_3 and N_2O were measured via Fourier transform infrared spectroscopy (FTIR; Vertex 80v spectrometer; Bruker, Germany). A custom cylindrical measurement cell (volume of circa (ca.): 1.7 L) was used. The cell features two potassium bromide windows on opposite sides to allow the passage of an infrared beam and a hole in the lid to insert the source. After preconditioning, the CAP device (turned on for 15 min) was inserted into the cell. After background determination, the source was turned on, and FTIR spectra were acquired every 15 s for 15 min. The same procedure was repeated for all three devices. The O_3 density was estimated from the main peak at approximately 1055 cm^{-1} and cross-checked with an overtone peak at 2120 cm^{-1} after the necessary baseline corrections were applied. Similarly, the concentration of N_2O was estimated from the main peak at 2240 cm^{-1}, and special care was taken to avoid interference with nearby CO_2 peaks. Additionally, O_3 was measured via an ozone analyzer (Figure S2 in Supplementary File).

2.3. Characterization of CAP-exposed saline

Viruses and bacteria were exposed to CAP in suspension. RONS production in an aqueous environment was also investigated by examining the presence of long-lived final products and monitoring the pH value in an exposed saline droplet. Drops of saline (30 µL; corresponding to the volume used for virus and bacteria testing) were placed on parafilm squares and treated with CAP for 120 min in triplicate. Approximate concentrations of nitrite (NO_2^-), nitrate (NO_3^-), and hydrogen peroxide (H_2O_2), as well as the pH, were semiquantitatively determined via indicator test strips (Quantofix nitrate/nitrite; Quantofix peroxide 100; and Lachner universal indicator strips for pH 0–12, respectively).

2.4. Bacteriology assessment

2.4.1. Assessment of P. aeruginosa viability

P. aeruginosa viability after CAP exposure was evaluated as previously described,[10] with slight modifications. Briefly, 1 × 1-cm parafilm squares were contaminated with a *P. aeruginosa* PAO1 strain suspension, which was adjusted to approximately 1×10^7 CFU/mL in 6 × 5-µL droplets. These squares were then placed in a Petri dish surrounded by two pieces of wet cotton wool to increase the humidity. The bacterial suspension was air-dried to stabilize the droplets on the parafilm surface for 15 min at room temperature and subsequently exposed to CAP for 1, 5, 10, and 30 min. The samples at each time point were tested in three technical and three independent biological replicates, along with the untreated control samples. Exposed *P. aeruginosa* cells (and untreated control samples) were collected from parafilm squares into 1 mL of saline in microtubes by vortexing. The counts (CFU/mL) were determined by decimal dilution of recovered suspensions inoculated directly on Luria–Bertani agar plates and incubated overnight at 37°C. The results were averaged and expressed as log CFU/mL with the standard error of the mean (SEM).

2.4.2. Visualization of P. aeruginosa cells via transmission electron microscopy

The morphology of *P. aeruginosa* PAO1 cells after CAP exposure was visualized via transmission electron microscopy (TEM), as previously reported,[54] with slight modifications. Briefly, bacterial cells exposed to CAP were visualized with negative staining via a JEOL JEM 1011 microscope (JEOL, Japan) operating at 80 kV. For negative staining, parlodion-carbon-coated grids were floated on 10 µL drops of each sample for 5 min. The grids were washed twice on a drop of water and negatively stained with 0.25% phosphotungstic acid (pH 7.4). The images are displayed in Figure 6 with scale bars of 500 nm.

2.4.3. Assessment of E. coli viability on 3D-printed objects

We also evaluated CAP-mediated surface decontamination via 3D-printed PETG that was exogenously contaminated with a wild-type *E. coli* suspension (~1×10^7 CFU/mL). As an additional control, the *E. coli* suspension was also spotted on other materials, including parafilm and P3 R filter tissue, for comparison with measurements performed in our earlier studies.[18,19] The samples were processed and

exposed to CAP generated by device 3, similar to that for *P. aeruginosa* (described in **Section 2.4.1.**).

2.5. Virologic assessment

The following virus strains and cell lines were used: (i) SARS-CoV-2 (hCoV-19/Czech Republic/NRL_6632_2/2020) was propagated in Vero E6 cells (ATCC CRL-1586) cultured in Dulbecco's modified Eagle medium (DMEM) supplemented with 2% fetal bovine serum (FBS); (ii) IAV (influenza A H1N1/California/07/2009; Diagnostic Hybrids, United States of America [USA]) was propagated in MDCK (ATCC CCL-34) cells cultured in influenza growth medium (DMEM supplemented with penicillin/streptomycin [Pen/Strep], 0.2% bovine serum albumin [BSA], 1 mM HEPES, 13.6 mM L-glutamine, 42 mg/L DEAE-Dextran, and 1 mg/L TPCK-Trypsin); (iii) HAdV (species C/type 2, ATCC VR-846) was propagated in A-549 cells (DSMZ ACC107) cultured in DMEM with 10% FBS and Pen/Strep; and (iv) HRV (species A/type 2, ATCC VR-482) was propagated in HeLa Ohio cells (both a kind gift of Heinrich Kowalski, Medical University of Vienna, Austria) cultured in DMEM with 10% FBS and Pen/Strep.

Parafilm squares (1 × 1 cm) inoculated with 30 µL of virus suspension (infectious dose: 10^3–10^6 IU/mL) were placed in a Petri dish surrounded by two pieces of wet cotton wool to increase the humidity. The virus-containing suspension was distributed across the parafilm surface in six droplets, air-dried for 15 min, and subsequently exposed to CAP for 10, 30, 90, and 120 min. Thereafter, the residual virus was recovered from the parafilm surface using 200 µL of phosphate-buffered saline (PBS), and the parafilm was thoroughly washed. To reduce the risk of bias, we implemented a control protocol for each sample, involving pipetting, 15 min of air-drying, mock exposure, and subsequent recovery. The recovered suspension was directly used for infecting permissive cells (specified above) to determine the infectious titer of each virus. All the data were generated from three biological replicates.

The SARS-CoV-2 titer was determined by diluting 20 µL of each sample in a 24-well plate containing 200 µL of cultivation medium in each well. The viral suspension was further diluted 1:10. Afterward, 300 µL of Vero E6 cells (2.5×10^5 per well) was added to the suspension and incubated for 4 h at 37°C and 5% CO_2. The mixture was subsequently overlaid with 500 µL of 3% carboxymethyl cellulose and incubated for 5 days at 37°C and 5% CO_2. The IAV titer was determined by pipetting 50 µL of each sample into a 24-well plate containing 300 µL of influenza growth medium (IGM) in each well. The viral suspension was further diluted 1:5. MDCK cells (1.8×10^5 per well, plated a day before the experiment) in a 24-well plate were washed once with PBS; 300 µL of IGM-containing serially diluted sample (1.5 µL of influenza A H1N1 virus in the first well) was added to the cells; the cells were then incubated for 1 h at 37°C and 5% CO_2. After 1 h, the cells were washed once with PBS; 300 µL of IGM was added to the cells; the medium was overlaid with 300 µL of 1.2% carboxymethyl cellulose; and the cells were incubated for 2 days at 37°C and 5% CO_2. For both SARS-CoV-2 and IAV, the infection was terminated by aspirating the medium. The cells were washed once with PBS, fixed, and stained with naphthalene black. After 45 min of incubation, the naphthalene black solution was aspirated, the cells were washed with water, and the resulting plaque-forming units (PFUs) were counted. The viral titer was expressed as PFU/mL. The 50% tissue culture infectious dose ($TCID_{50}$) of HAdV and HRV was determined by inoculating serially diluted (10-fold) samples (10 µL/well) in 96-well microtiter plates, in which A549 and HeLa Ohio cells were seeded, respectively. The infected cells were incubated at 37°C in a 5% CO_2 incubator for 5 (HRV) or 7 days (HAdV). The cytopathic effect (CPE) was visualized via a crystal violet assay as previously described.[20] The Spearman–Kärber method[21,22] was used to calculate the respective infectious titers (IU/mL).

Quantitative polymerase chain reaction (qPCR) was performed to determine the number of recovered virus genome copies. For SARS-CoV-2, a commercial kit (gb Sarbeco E, Cat. no. 3227--500; Generi Biotech, Czech Republic) was used in accordance with the manufacturer's instructions. IAV genome copies were determined via the Luna Universal Probe One-Step RT-qPCR Kit (New England Biolabs, USA), as previously described.[55] Recovered HAdV and HRV genome copies were measured via previously described protocols: HAdV (type C)[23,24] and HRV (multiplex).[28]

3. Results

3.1 CAP composition produced by the 3D-printed devices

The concentrations of NO and NO_2 in the gaseous environment of devices 1, 2, and 3 were measured during the generation of CAP over 120 min. While NO levels remained undetectable in all cases (data not disclosed), NO_2 levels displayed an obvious difference between optimized devices 2/3 and the original device 1, suggesting that the optimized devices are more efficient in producing NO_2 (Figure 2).

The concentrations of O_3 and N_2O obtained from the FTIR spectra are depicted in Figure 3 as a function of the source operating time. The gradual increase in the concentration measured inside the reactor suggested stable continuous production of O_3 and N_2O by the devices. Device 1 appeared to be less efficient in the production

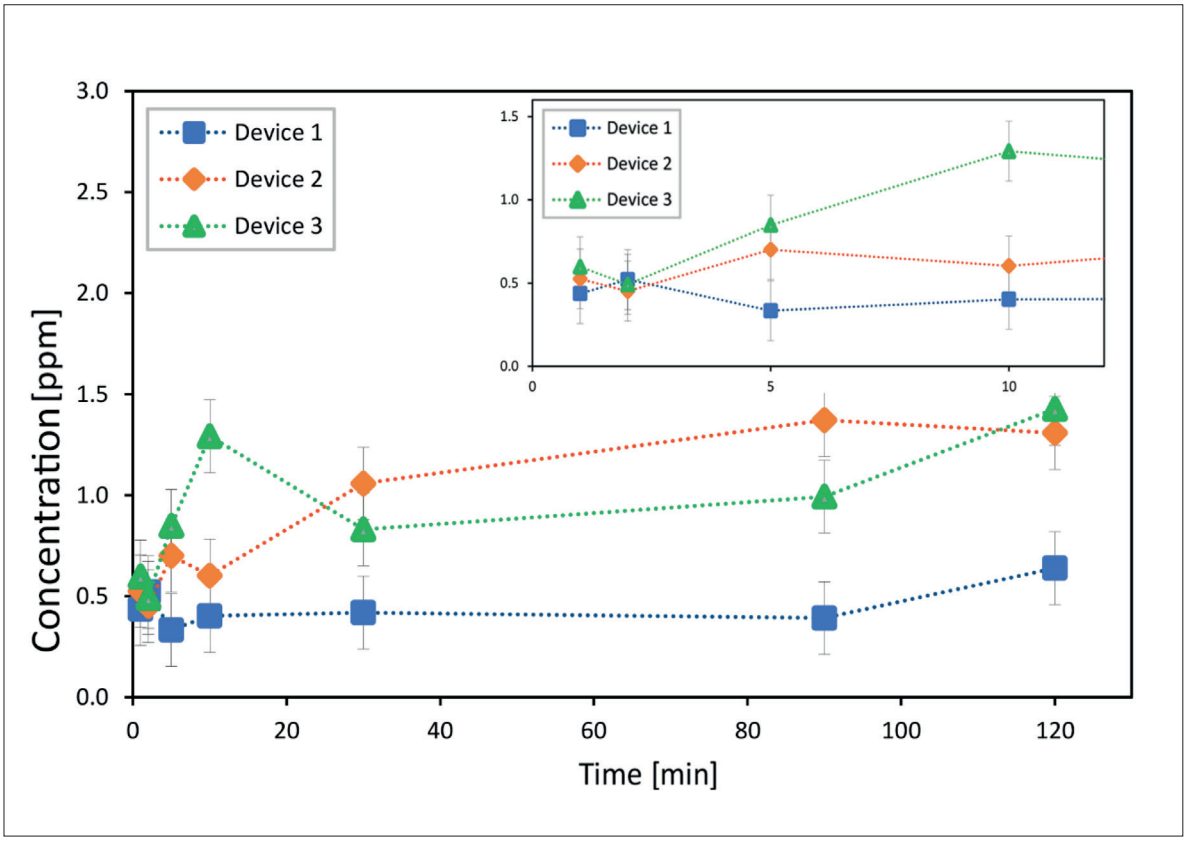

Figure 2. Concentration of NO_2 in the gaseous environment of devices 1, 2, and 3 measured over 120 min. Concentrations of NO_2 in devices 1, 2, and 3 in the first 10 min (inset). The concentration of NO_2 increases due to its accumulation in the gaseous environment of the devices, with the highest concentration noted for devices 2 and 3. The results are averaged from three independent measurements and depicted in ppm ± standard error of the mean.

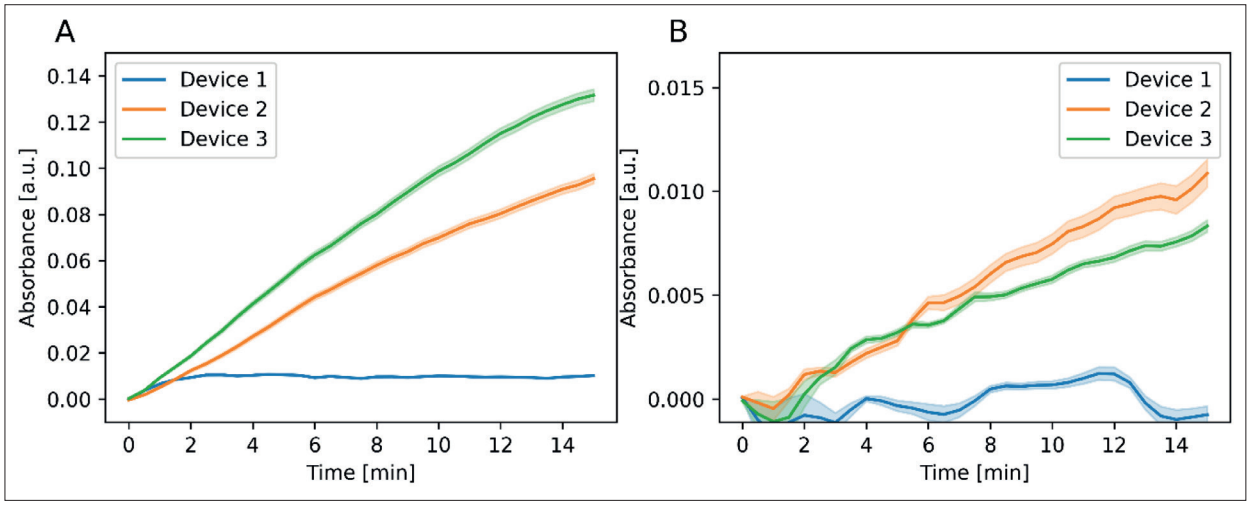

Figure 3. Concentration of O_3 (A) and N_2O (B) in the gaseous environment of devices 1, 2, and 3, measured over 15 min of operation in a closed reactor. Spectra were sampled every 30 s, and the concentration of gases was determined by integrating the area under the corresponding absorption peaks, after correcting for baseline drifting. Due to unavailable cross sections, the measure is reported in arbitrary units (a.u.), which are proportional to the actual density. The highlighted areas represent 1σ uncertainty, estimated from spectral analysis. The gradual increase reflects the production and accumulation of measured gases, with devices 2 and 3 producing more reactive species than device 1.

of both species, while the results of devices 2 and 3 were comparable (Figure 3). Similar results were obtained via an ultraviolet (UV)-100 ozone analyzer, whereby device 1 produced significantly less O_3 compared to the optimized devices (Figure S2 in Supplementary File).

To evaluate the CAP environment to which the pathogens were exposed, we assessed a drop of saline (representing the aqueous environment) exposed to CAP in the device chambers. The measured pH value indicated that the aqueous environment was highly acidic after treatment by all the devices. Specifically,

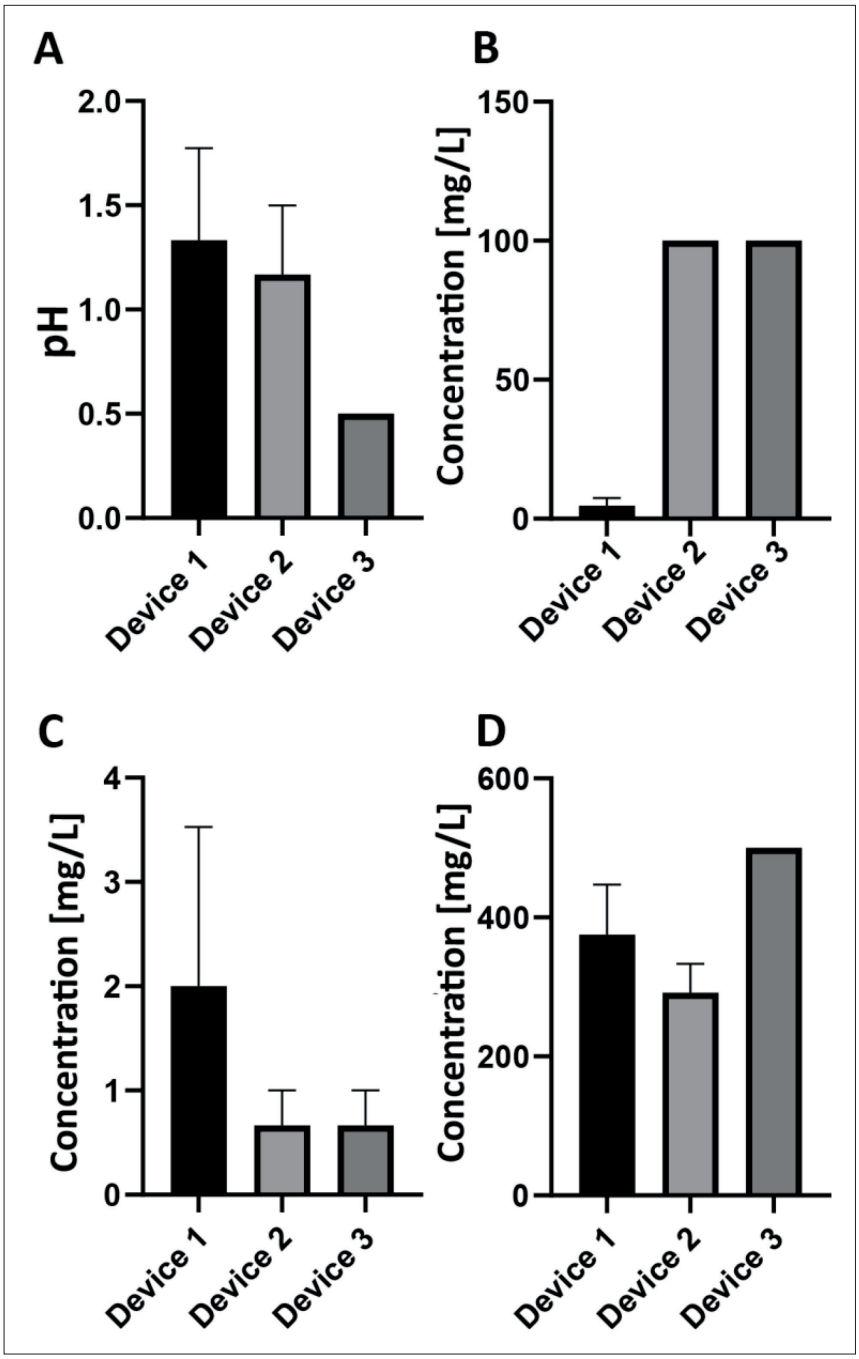

Figure 4. Reactive oxygen and nitrogen species (RONS) generated in saline after exposure (of 30 µL saline) to 3D-printed cold atmospheric plasma (CAP) in devices 1, 2, and 3 for 120 min. The pH (A) and concentrations of H_2O_2 (B), NO_2^- (C), and NO_3^- (D) were measured after 120 min of exposure. Results were averaged from three independent measurements and are presented as the mean and corresponding standard error of the mean. Values without depicted error bars were identical across all measurements (i.e., standard error of the mean = 0). Abbreviation: c: Concentration.

device 1 reported a pH of approximately 1.3, whereas optimized devices 2 and 3 reported pH values of 1.2 and 0.5, respectively (Figure 4A). H_2O_2 was almost absent when the original device 1 was used, whereas optimized devices 2 and 3 reported H_2O_2 concentrations of up to 100 mg/L (Figure 4B). In general, the concentration of NO_2^- appeared to be relatively low (<4 mg/L) for all devices. The concentration of NO_2^- was, on average, the highest for device 1, approximately twice as high compared to the optimized devices 2 and 3. However, given the large SEM, the values obtained for all devices can be considered comparable (Figure 4C). NO_3^- levels were relatively high for all the tested devices (350–500 mg/L), with the highest value obtained for device 3 (500 mg/L) (Figure 4).

3.2. Viability of *P. aeruginosa* cells after exposure to CAP

P. aeruginosa PAO1 cells on parafilm squares were exposed to CAP from the three 3D-printed devices for 1, 5, 10, and 30 min. The results indicated that original device 1 exhibited a weaker microbicidal effect compared to optimized devices 2 and 3 (Figure 5). In contrast, devices 2 and 3, which were decontaminated with parafilm squares, displayed 100% efficiency after only 1 min of CAP exposure. Device 1 reduced *P. aeruginosa* contamination by approximately 1, 2, and 5 log CFU/L after 1, 5, and 10 min of CAP exposure, respectively, followed by complete decontamination of the parafilm squares only after 30 min of CAP exposure.

3.3. Morphology of *P. aeruginosa* cells after exposure to CAP

A visualization of *P. aeruginosa* PAO1 cells exposed to the three different CAP-generating devices via TEM is depicted in Figure 6. The control sample (Figure 6A) displayed intact rod-shaped cells with flagella. Device 1 did not cause any significant changes in cell morphology after 1 min of exposure (Figure 6B). However, after 5 min, visible dimming of the cell surface indicated incipient cell membrane damage (Figure 6C), which progressed to severely disturbed cell surface features after 10 min of exposure (Figure 6D). In contrast, 1 min of exposure to devices 2 and 3 (Figure 6E and H, respectively) resulted in changes in the cell surface; 5 min of exposure induced severe damage to the cell membrane, as indicated by thick dark demarcations (Figure 6F and I, respectively); and 10 min of exposure led to rupture of the cell membrane

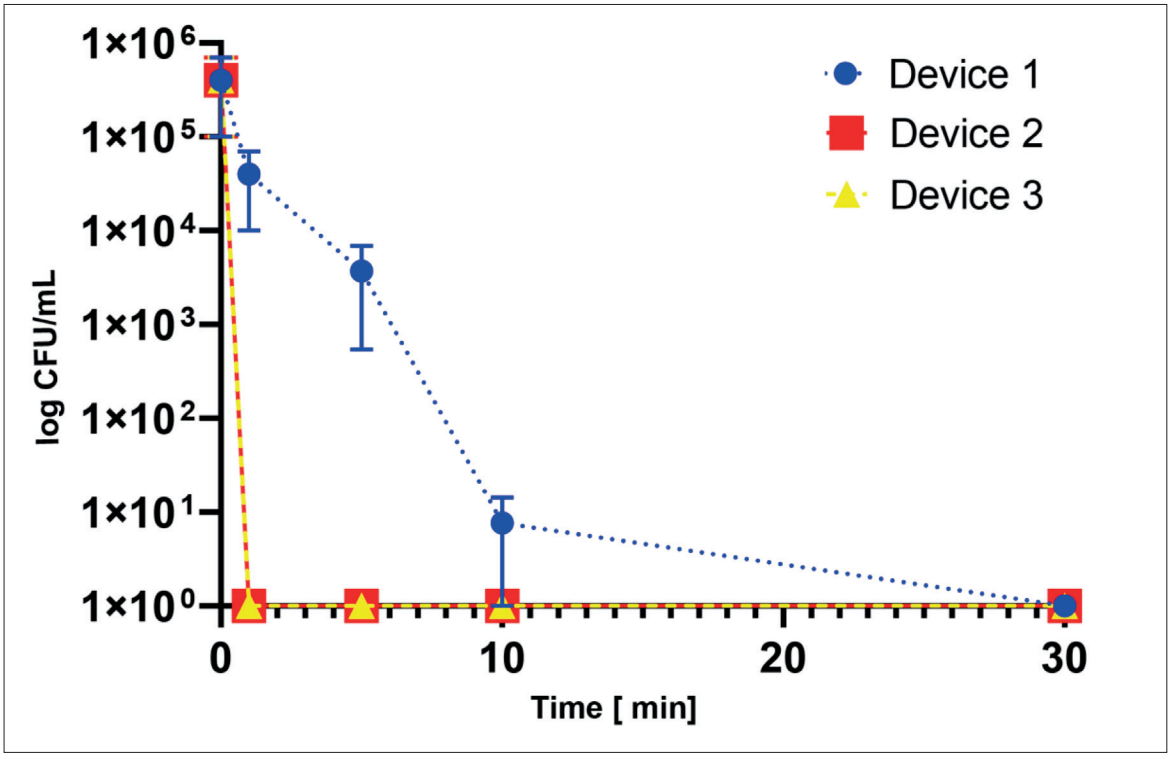

Figure 5. Effects of three 3D-printed cold atmospheric plasma (CAP)-generating devices on the viability of *P. aeruginosa* PAO1 cells. The bacteria were exposed to CAP for 1–30 min. Survival was determined by assessing the colony-forming units (CFUs) and plotting them as log CFU/mL.

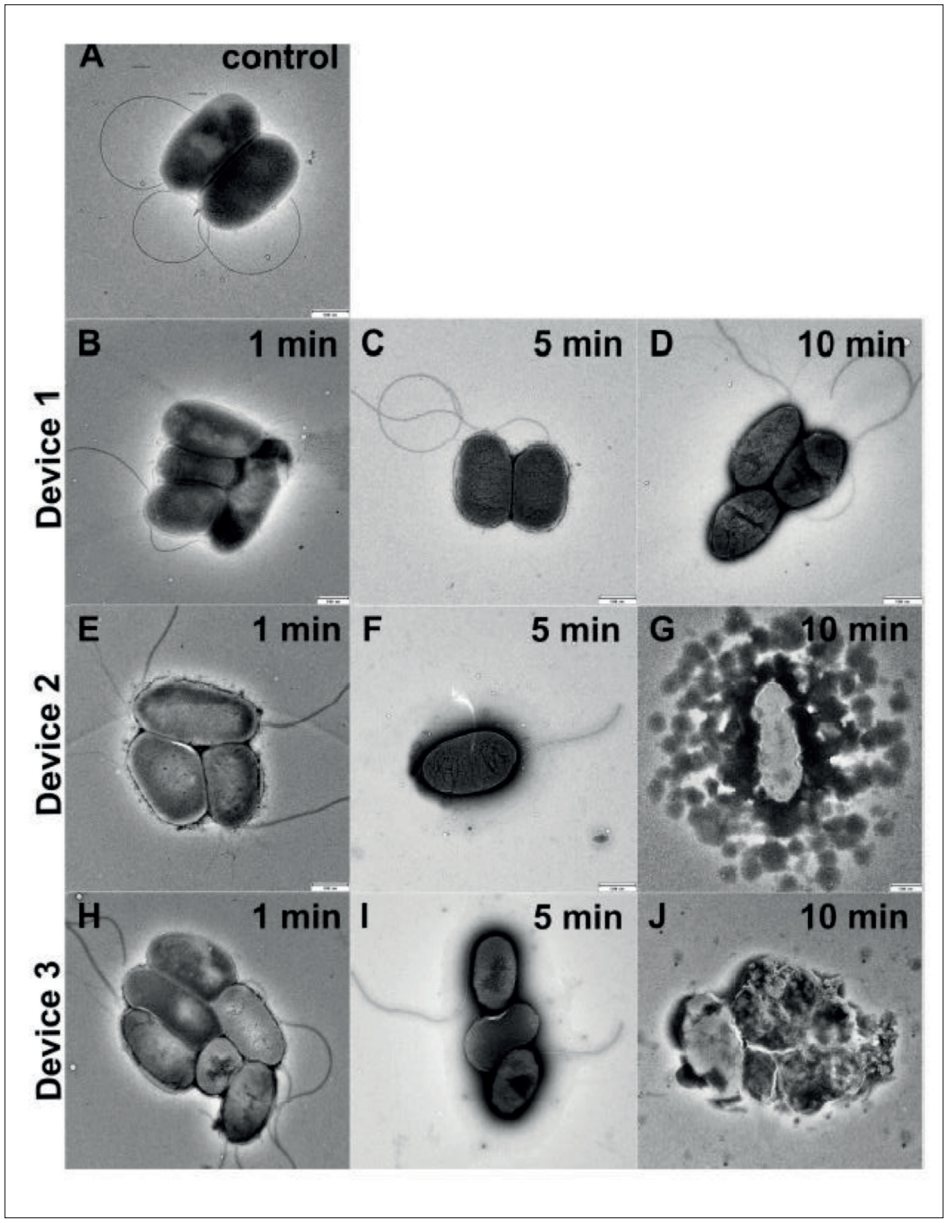

Figure 6. Differential effects of three different 3D-printed cold atmospheric plasma (CAP)-generating devices on the morphology of *Pseudomonas aeruginosa* PAO1 cells visualized by transmission electron microscopy (TEM). As observed, increasing the duration of exposure to CAP damages the cell membrane, leading to cell disruption and content leakage. TEM images of cells in (A) the unexposed control sample; (B) device 1, exposure for 1 min; (C) device 1, exposure for 5 min; (D) device 1, exposure for 10 min; (E) device 2, exposure for 1 min; (F) device 2, exposure 5 min; (G) device 2, exposure for 10 min; (H) device 3, exposure for 1 min; (I) device 3, exposure for 5 min; and (J) device 3, exposure for 10 min. Scale bars: 500 nm. Magnification: XXX.Will be done

(Figure 6G and J, respectively). Notably, complete leakage of the cell contents was visible after 10 min of CAP exposure via device 2 (Figure 6G).

3.4. CAP exposure reduces viral infectivity and compromises particle integrity

We directly compared the virucidal effects of the three devices by exposing virus-contaminated parafilm squares to CAP for 10, 30, 90, and 120 min. SARS-CoV-2 infectivity in permissive cells was completely eliminated by optimized devices 2 and 3 after 90 min of exposure, whereas original device 1 required 120 min (Figure 7A; Table S1 in Supplementary File). Viral genome copy numbers determined by qPCR demonstrated that the optimized devices could effectively eliminate over 99.5% of SARS-CoV-2 RNA after 90 min, whereas the original device reduced the RNA level by 96% after only 120 min (Figure 8A; Table S1 in Supplementary File). Hence, the

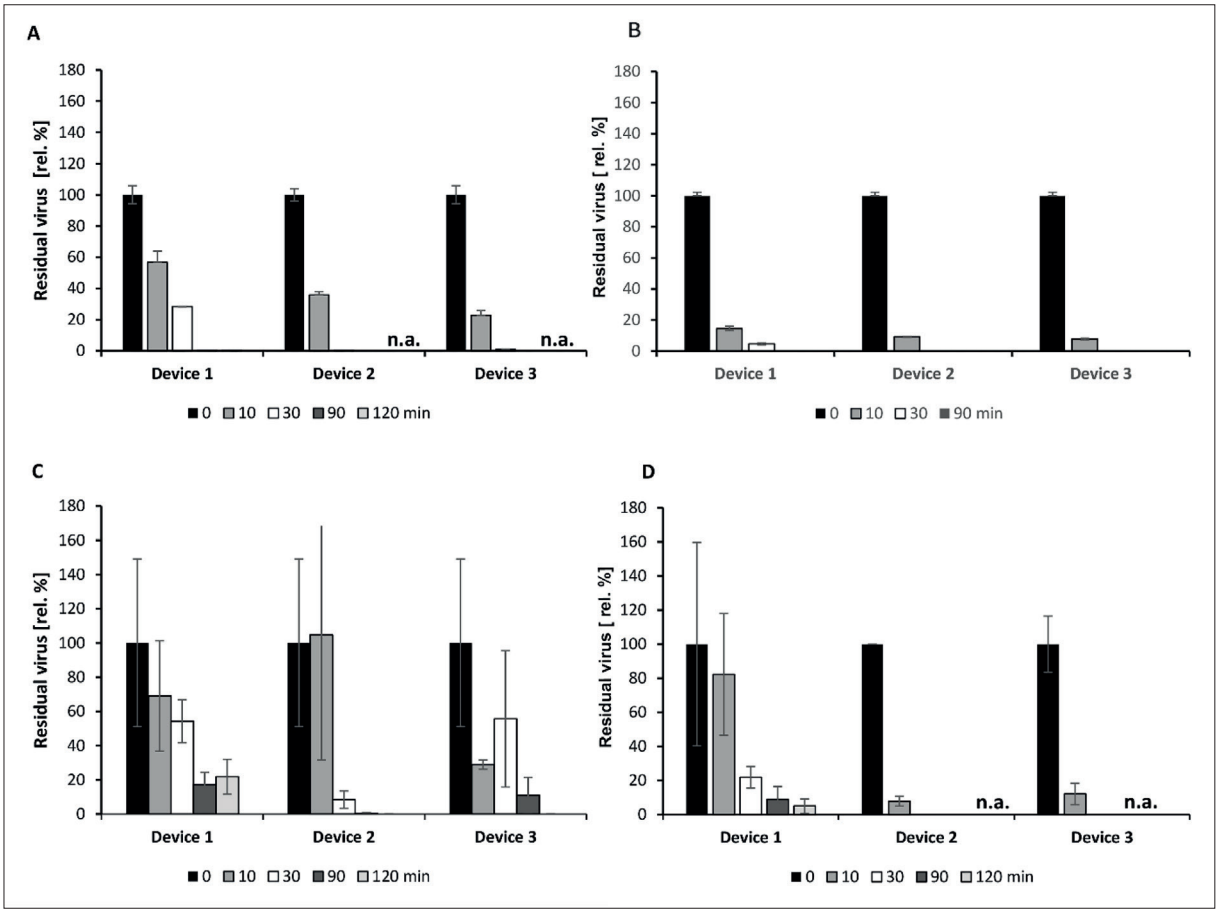

Figure 7. Virus infectivity reduction after cold atmospheric plasma (CAP) treatment for (A) SARS-CoV-2; (B) influenza A H1N1; (C) adenovirus; and (D) rhinovirus. The viral inoculum was spotted on parafilm, air-dried, and subsequently exposed to CAP for specific durations. The residual infectivity of the viruses was determined in cell culture, and the results are plotted as relative percentages to untreated control samples. The average of three biological replicates with the standard error of the mean are displayed for all the measurements. Increasing the duration of CAP exposure resulted in a progressive reduction in viral infectivity, and optimized devices 2 and 3 were superior to original device 1. If complete elimination of infectivity was achieved, residual infectivity was not analyzed at longer exposure times (n.a.).

virucidal effect of the optimized devices occurred more rapidly, with device 3 exhibiting slightly higher efficiency than device 2.

All the tested 3D-printed devices completely abrogated the infectivity of IAV. The original device required 90 min to completely eliminate the infectious capacity of IAV, whereas the optimized devices required only 30 min (Figure 7B; Table S2 in Supplementary File). Device 3 demonstrated significantly better performance in terms of particle destruction than did device 2 (Figure 8B; Table S2 in Supplementary File). The inferior performance of the original device was also documented by qPCR analysis.

Following CAP treatment using the optimized devices, HRV infectivity decreased over time, reaching complete elimination after 30 min of exposure, whereas the original device was unable to completely inactivate HRV even after 120 min (Figure 7D; Table S4 in Supplementary File). The number of viral genome copies decreased by approximately 75% after 30 min of treatment with devices 2 or 3, whereas device 1 produced similar results after only 120 min (Figure 8D; Table S4 in Supplementary File).

As expected, the HAdV samples were more resistant to treatment with CAP than the tested RNA viruses were and required longer exposures to decrease their infectivity. The optimized devices facilitated the complete elimination of the HAdV infectious capacity after 120 min, whereas the original device only reduced the infectivity by approximately 80% after the same exposure time (Figure 7C; Table S3). Viral genome copies determined by validated qPCR[56] were reduced

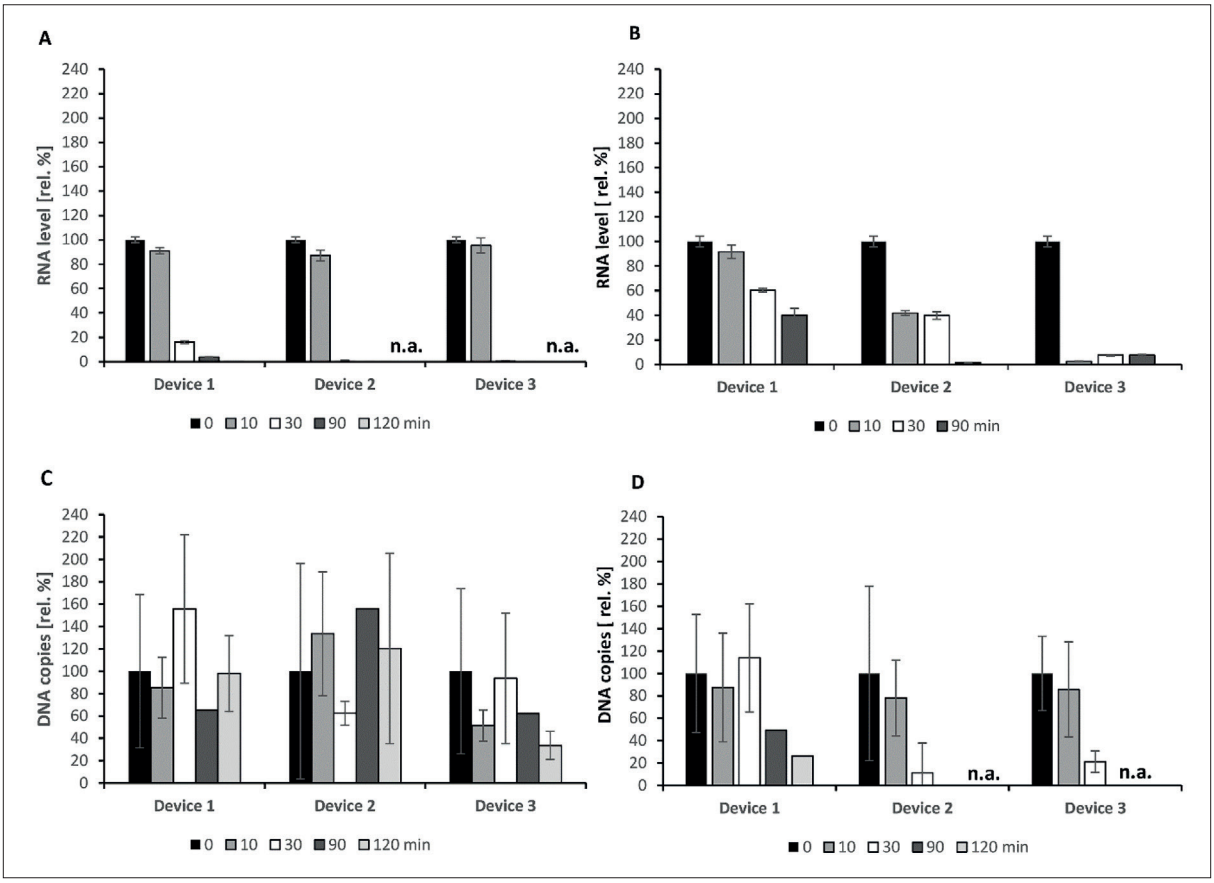

Figure 8. Viral genome copy reduction after cold atmospheric plasma (CAP) treatment for (A) SARS-CoV-2; (B) influenza A H1N1; (C) adenovirus; and (D) rhinovirus. The viral inoculum was spotted on parafilm, air-dried, and subsequently exposed to CAP for specific durations. Residual virus nucleic acid copies (genome equivalents) were determined via quantitative polymerase chain reaction (qPCR). The results are plotted as relative percentages to untreated control samples. The average of three biological replicates with the standard error of the mean are displayed for all the measurements. Increasing the duration of CAP exposure resulted in a progressive reduction of viral copy numbers, and optimized devices 2 and 3 were superior to original device 1. If complete elimination of infectivity was achieved, residual virus nucleic acid copies were not analyzed at longer exposure times (n.a.).

at a slower pace than infectivity (Figure 8C; Table S3). Additionally, the efficiency of device 3 was superior to that of device 2.

3.5. CAP-mediated decontamination of 3D-printed material

To assess the ability and efficacy of CAP in decontaminating 3D-printed materials, a proof-of-concept experiment was conducted in which 3D-printed PETG contaminated with *E. coli* was tested. Consistent with our earlier findings, exposure to CAP facilitated complete inactivation of the bacteria within 5 min (Figure S3).

4. Discussion

Cold atmospheric plasma (CAP) is regarded as a groundbreaking disinfection technology with vast potential for decontaminating various sensitive surfaces from pathogens. It features high effectiveness, nontoxic byproducts, minimal side effects, and operates under favorable conditions, including low temperatures. CAP can be used continuously and is amenable to human applications. The effects of CAP on biological samples depend on the plasma-generating device used, and 3D printing offers the required flexibility to facilitate the production of optimized instruments. Production is regulated by several critical factors, including construction (geometry) and technical parameters, such as applied power, voltage, and waveform. Furthermore, ambient conditions during application, such as the atmospheric composition, humidity, and pressure, influence the efficacy of CAP.[29] Hence, improving the design of 3D-printed devices, operating conditions, and parameters for the practical application of CAP is essential.

In this study, we examined the efficiency of three CAP devices for selecting enveloped and nonenveloped viruses and a clinically important gram-negative bacterium. The three devices were produced via a 3D printer and could be easily adjusted to the desired size, shape, and inner chamber geometry. Along with the original device used in earlier studies, we tested two optimized versions containing a closed chamber that produces a more densely concentrated particle environment. These versions incorporated a tubular "volcano" design, which accurately directs particle flow toward the sample. Another feature of potential improvement was the use of two electric discharges in parallel (Figure 1). All three devices demonstrated good performance in decontaminating surfaces from pathogens, but the devices displayed different efficiencies defined by the time of exposure to CAP required for inactivation. According to the parameters recorded, optimized devices 2 and 3 were superior to the original device 1 in all analyses performed, including the reduction in infectivity, nucleic acid degradation, and external membrane damage in relation to the duration of CAP exposure.

To characterize the CAP composition produced by individual devices, we analyzed the concentration of RONS accumulated in gaseous (Figures 2 and 3) and aqueous (Figure 4) environments. The optimized devices yielded relatively high concentrations of O_3, N_2O, and NO_2 in the gaseous environment and relatively high H2O2 concentrations in the saline solution. The pH of the exposed saline drop was generally low, with the lowest value generated by device 3 (pH 0.5). All the tested devices yielded comparable concentrations of NO_3^- and NO_2^- in the aqueous environment (based on SEM images). The results indicate that the use of closed-chamber formats (devices 2 and 3) led to changes in the CAP atmosphere, thereby increasing decontamination efficiency. Notably, the inclusion of an additional discharge electrode (device 2) had a minimal impact on decontamination efficiency.

The antibacterial properties of CAP apparently correlate with the concentration of RONS produced by the devices. This notion is reflected by the greater efficacy of optimized devices 2 and 3 in eliminating the viability of *P. aeruginosa* almost instantaneously, whereas device 1 required 30 min for the same effect (Figure 5). In this study, bacteria suspended in saline solution during CAP treatment suggested that RONS, specifically H2O2, may play a crucial role in antibacterial efficacy, especially in direct bacterial exposure to CAP.[56] This assumption is supported by the considerably greater H_2O_2 concentration in the CAP-exposed saline drop generated by devices 2 and 3 (Figure 4). The antimicrobial effect of RONS is well described in the literature,[57–59] and their presence has also been validated in a gaseous environment (Figures 2 and 3). However, H_2O_2 likely played a significant role in our analysis of bacterial inactivation in saline solution because of the low solubility of RONS in water. In contrast to the long CAP exposure times required for virus inactivation (up to 120 min; Figures 7 and 8), bacterial cells were inactivated by devices 2 and 3 within 1 min (Figure 5), where evaporation of the liquid is not expected to be a relevant factor. The antibacterial effect of CAP was also reflected by a greater degree of physical damage, including membrane impairment and cell content leakage, as visualized via TEM. This damage was more rapidly inflicted by devices 2 and 3 (Figure 6). CAP exposure damages the bacterial cell wall, leading to high levels of oxidative stress and cell membrane rupture, as well as bacterial cell death due to DNA damage.[60–64] Many studies have reported pronounced antibacterial effects of CAP generated in gaseous environments (i.e., containing a single RONS or a combination of RONS), which produces H_2O_2 and NO_2^- in aqueous environments.[58,65–69]

The antiviral efficiency exhibited a similar trend as described above, with devices 2 and 3 outperforming device 1 in all the assays performed (Figures 7 and 8; Tables S1–S4). Given the long exposure time required for viral inactivation (up to 120 min), significant evaporation of the liquid surrounding the viral particles is likely. Hence, both RONS detected in a gaseous environment and H_2O_2 detected at high concentrations in the aqueous environment upon treatment by devices 2 and 3 appear to play a relevant role in the virucidal effects observed. Viral infectivity decreased gradually over the CAP exposure time, and complete elimination was generally achieved more rapidly with the optimized devices. The reduction in viral genome copy number, which was analyzed to monitor the physical integrity of virus particles, exhibited the same trend, albeit more slowly, indicating that infectivity was diminished before complete particle disintegration. This trend was previously reported by us[19] and supports the notion that perfect virus fitness viability is required for infectivity but does not directly correlate with particle integrity. Repeated measurements often reveal fluctuating readouts, especially for HAdV and HRV, at shorter CAP exposure times. This was also the case for the control measurements before CAP exposure, thus reflecting the biological complexity of the experimental system. In line with previous observations,[70] enveloped RNA viruses (SARS-CoV-2 and IAV in the present study) and the nonenveloped virus HRV were more rapidly inactivated by CAP, whereas HAdV displayed a greater degree of stability. It has been previously reported that both enveloped and nonenveloped viruses can be inactivated by reactive plasma particles through oxidative damage to proteins, viral envelopes (if present), and nucleic acids.[71]

Various CAP experiments have suggested that O_3 might be the principal RONS responsible for viral inactivation.[72–74] whereas other observations highlighted the role of H_2O_2 and low pH[75] in the mechanism of CAP-mediated viral inactivation. Mentel et al.[76] examined the effects of H_2O_2 on different viruses at various concentrations and H_2O_2 exposure times. These findings indicate that all viruses tested (CoV strain 229E, influenza A and B viruses, HAdV, and HRV 1A, 1B, and type 7) were rendered inactive by 3% H_2O_2 within 1–30 min. In agreement with our data, the enveloped RNA viruses (SARS-CoV-2 and IAV) were most susceptible to the effects of H_2O_2, whereas HAdV was most resistant.[76] H_2O_2 is a powerful oxidizing agent that causes genetic damage, impairing the replicative capacity of both DNA and RNA viruses.[77] The mechanism of action of H_2O_2 involves attacking carbon double bonds in nucleosides or removing hydrogen atoms, leading to single- or double-strand breaks in DNA or RNA.[77,78] Additionally, CAP-derived RONS affect the receptor-binding region of the SARS-CoV-2 spike (S) protein, which is essential for its attachment to host cells and infectivity.[79,80] Consistent with published data, we observed a substantial improvement in both the microbicidal and virucidal efficiency of devices that produced O_3 and H_2O_2 at relatively high concentrations and more efficiently induced pH acidification.

The impact of the device on decontamination-related parameters is relevant not only from a scientific standpoint but also for its practical application in daily use. The device has the potential to be employed for decontaminating large areas and various sensitive materials and objects that are impossible or very difficult to disinfect via other methods. Specifically, one of our ongoing research objectives is to decontaminate children's plush toys, particularly for their use in stem cell transplant wards. Moreover, adapting the device for surface decontamination of 3D-bioprinted scaffolds for medical applications is also conceivable. In the present study, we demonstrated the basic applicability and efficacy of CAP for the decontamination of 3D-printed PETG, and the observations can expectedly be extended to a variety of other bioprinted materials.

In this context, safety is a concern due to the high voltages of several kVs used in the device. As outlined above, the device presented here is robust and mechanically resistant. The HV wires are well embedded in the device, and the separating air layer significantly exceeds the effective electrical strength. In addition, a significant advantage of the HV source used is its low current output. While capable of delivering HV, it generates only low currents on the order of 100 μA, well below the safety limit. In the event of direct contact with the HV wires, the voltage drops immediately, resulting in only a mild sensation of electrostatic charge for the person involved.

5. Conclusion

In summary, our observations indicate substantially enhanced CAP efficiency against all pathogens tested when using 3D-printed devices with closed reaction chambers and a "volcano" design to guide reactive particles. The optimized parameters facilitated complete inactivation with shorter CAP exposure times, potentially due to the increased accumulation of certain RONS in the gaseous environment or H_2O_2 in the aqueous environment. The findings highlight the potential of CAP as an easily applicable, inexpensive, and soft technique for decontaminating sensitive surfaces from viral and bacterial pathogens, particularly when other technical approaches based on heat exposure or antimicrobial liquids cannot be readily applied.

Acknowledgments

None

Funding

This study was supported by the FWF I 5293-B/GACR GF21-39019 L grant and by the National Institute Virology and Bacteriology project (Programme EXCELES; Project No. LX22NPO5103), funded by the European Union (EU) under the Next Generation EU initiative.

Conflict of interest

The authors declare that the research was conducted in the absence of any commercial or financial relationships that could be construed as potential conflicts of interest.

Author contributions

Conceptualization: Klára Obrová, Eva Vaňková

Formal analysis: Asma Bouazizi, Klára Obrová, Anna Machková, Josef Khun, Romana Hadravová, Jan Hodek, Lucie Ulrychová, Leonardo Zampieri, Fabio Avino

Funding acquisition: Klára Obrová, Abdelhalim Trabelsi, Jan Weber, Ivo Furno, Vladimír Scholtz, Thomas Lion

Investigation: Asma Bouazizi, Klára Obrová, Anna Machková, Josef Khun, Romana Hadravová, Jan Hodek, Lucie Ulrychová, Leonardo Zampieri, Fabio Avino

Methodology: Klára Obrová, Eva Vaňková

Project administration: Klára Obrová, Eva Vaňková

Supervision: Klára Obrová, Abdelhalim Trabelsi, Jan Weber, Ivo Furno, Vladimír Scholtz, Thomas Lion
Visualization: Asma Bouazizi, Klára Obrová, Anna Machková, Josef Khun, Romana Hadravová, Jan Hodek, Lucie Ulrychová, Leonardo Zampieri, Fabio Avino
Writing – original draft: Asma Bouazizi
Writing – review & editing: All authors

Ethics approval and consent to participate

Not applicable.

Consent for publication

Not applicable.

Availability of data

The data presented in this study are available upon request from the corresponding author.

References

1. Fernández A, Noriega E, Thompson A. Inactivation of *Salmonella enterica* serovar Typhimurium on fresh produce by cold atmospheric gas plasma technology. *Food Microbiol*. 2013;33(1):24-29. doi: 10.1016/j.fm.2012.08.007
2. Baier M, Görgen M, Ehlbeck J, Knorr D, Herppich WB, Schlüter O. Non-thermal atmospheric pressure plasma: Screening for gentle process conditions and antibacterial efficiency on perishable fresh produce. *Innov Food Sci Emerg Technol*. 2014;22:147-157. doi: 10.1016/j.ifset.2014.01.011
3. Hertwig C, Reineke K, Ehlbeck J, Knorr D, Schlüter O. Decontamination of whole black pepper using different cold atmospheric pressure plasma applications. *Food Control*. 2015;55:221-229. doi: 10.1016/j.foodcont.2015.03.003
4. Choi S, Puligundla P, Mok C. Corona discharge plasma jet for inactivation of *Escherichia coli* O157:H7 and *Listeria monocytogenes* on inoculated pork and its impact on meat quality attributes. *Ann Microbiol*. 2016;66(2):685-694. doi: 10.1007/S13213-015-1147-5
5. Oh YJ, Song AY, Min SC. Inhibition of *Salmonella typhimurium* on radish sprouts using nitrogen-cold plasma. *Int J Food Microbiol*. 2017;249:66-71. doi: 10.1016/J.IJFOODMICRO.2017.03.005
6. Van Gils CAJ, Hofmann S, Boekema BKHL, Brandenburg R, Bruggeman PJ. Mechanisms of bacterial inactivation in the liquid phase induced by a remote RF cold atmospheric pressure plasma jet. *J Phys D Appl Phys*. 2013;46(17):175203. doi: 10.1088/0022-3727/46/17/175203
7. Alkawareek MY, Algwari QT, Laverty G, et al. Eradication of *Pseudomonas aeruginosa* Biofilms by Atmospheric Pressure Non-Thermal Plasma. *PLoS One*. 2012;7(8):44289. doi: 10.1371/JOURNAL.PONE.0044289
8. Laroussi M. Low-temperature plasmas for medicine? *IEEE Trans Plasma Sci*. 2009;37(6 PART 1):714-725 doi: 10.1109/TPS.2009.2017267
9. Moreau M, Orange N, Feuilloley MGJ. Non-thermal plasma technologies: new tools for bio-decontamination. *Biotechnol Adv*. 2008;26(6):610-617. doi: 10.1016/j.biotechadv.2008.08.001
10. Kong MG, Kroesen G, Morfill G, et al. Plasma medicine: an introductory review. *New J Phys*. 2009;11(11):115012. doi: 10.1088/1367-2630/11/11/115012
11. Nosenko T, Shimizu T, Morfill GE. Designing plasmas for chronic wound disinfection. *New J Phys*. 2009;11(11):115013. doi: 10.1088/1367-2630/11/11/115013
12. Heinlin J, Isbary G, Stolz W, et al. Plasma applications in medicine with a special focus on dermatology. *J Eur Acad Dermatology Venereol*. 2011;25(1):1-11. doi: 10.1111/j.1468-3083.2010.03702.x
13. Von Woedtke T, Haertel B, Weltmann KD, Lindequist U. Plasma pharmacy - physical plasma in pharmaceutical applications. *Pharmazie*. 2013;68(7):492-498. doi: 10.1691/ph.2013.6521
14. von Woedtke T, Reuter S, Masur K, Weltmann KD. Plasmas for medicine. *Phys Rep*. 2013;530(4):291-320. doi: 10.1016/j.physrep.2013.05.005
15. Theus AS, Ning L, Kabboul G, et al. 3D bioprinting of nanoparticle-laden hydrogel scaffolds with enhanced antibacterial and imaging properties. *iScience*. 2022;25(9):104947. doi: 10.1016/j.isci.2022.104947
16. Liu H, Xing F, Yu P, et al. A review of biomacromolecule-based 3D bioprinting strategies for structure–function integrated repair of skin tissues. *Int J Biol Macromol*. 2024;268(Pt 2). doi: 10.1016/J.IJBIOMAC.2024.131623
17. Dubey A, Vahabi H, Kumaravel V. Antimicrobial and Biodegradable 3D Printed Scaffolds for Orthopedic Infections. *ACS Biomater Sci Eng*. 2023;9(7):4020-4044. doi: 10.1021/acsbiomaterials.3c00115
18. Vaňková E, Kašparová P, Khun J, et al. Polylactic acid as a suitable material for 3D printing of protective masks in times of COVID-19 pandemic. *PeerJ*. 2020;8:1-20. doi: 10.7717/peerj.10259
19. Obrová K, Vaňková E, Sláma M, et al. Decontamination of high-efficiency mask filters from respiratory pathogens including SARS-CoV-2 by non-thermal plasma. *Front Bioeng Biotechnol*. 2022;10(February):1-13. doi: 10.3389/fbioe.2022.815393

20. Aboubakr HA, Williams P, Gangal U, et al. Virucidal effect of cold atmospheric gaseous plasma on feline calicivirus, a surrogate for human norovirus. *Appl Environ Microbiol*. 2015;81(11):3612-3622. doi: 10.1128/AEM.00054-15

21. Ahlfeld B, Li Y, Boulaaba A, et al. Inactivation of a foodborne norovirus outbreak strain with nonthermal atmospheric pressure plasma. *MBio*. 2015;6(1). doi: 10.1128/MBIO.02300-14

22. Bae SC, Park SY, Choe W, Ha S Do. Inactivation of murine norovirus-1 and hepatitis A virus on fresh meats by atmospheric pressure plasma jets. *Food Res Int*. 2015;76: 342-347. doi: 10.1016/j.foodres.2015.06.039

23. Lacombe A, Niemira BA, Gurtler JB, et al. Nonthermal inactivation of norovirus surrogates on blueberries using atmospheric cold plasma. *Food Microbiol*. 2017;63:1-5. doi: 10.1016/j.fm.2016.10.030

24. Nayak G, Aboubakr HA, Goyal SM, Bruggeman PJ. Reactive species responsible for the inactivation of feline calicivirus by a two-dimensional array of integrated coaxial microhollow dielectric barrier discharges in air. *Plasma Process Polym*. 2018;15(1):1700119. doi: 10.1002/PPAP.201700119

25. Mohamed H, Nayak G, Rendine N, et al. Non-thermal plasma as a novel strategy for treating or preventing viral infection and associated disease. *Front Phys*. 2021;9(June):1-25. doi: 10.3389/fphy.2021.683118

26. Assadi I, Guesmi A, Baaloudj O, et al. Review on inactivation of airborne viruses using nonthermal plasma technologies: from MS2 to coronavirus. *Environ Sci Pollut Res*. 2022;29:4880-4892. doi: 10.1007/s11356-021-17486-3

27. Filipić A, Gutierrez-Aguirre I, Primc G, Mozetič M, Dobnik D. Cold Plasma, a new hope in the field of virus inactivation. *Trends Biotechnol*. 2020;38(11):1278-1291. doi: 10.1016/j.tibtech.2020.04.003

28. Scholtz V, Vaňková E, Kašparová P, Premanath R, Karunasagar I, Julák J. Nonthermal plasma treatment of ESKAPE pathogens: a review. *Front Microbiol*. 2021;12(October):1-20. doi: 10.3389/fmicb.2021.737635

29. Scholtz V, Julák J, Kříha V. The microbicidal effect of low-temperature plasma generated by corona discharge: comparison of various microorganisms on an agar surface or in aqueous suspension. *Plasma Process Polym*. 2010; 7(3-4):237-243. doi: 10.1002/ppap.200900072

30. Mai-Prochnow A, Murphy AB, McLean KM, Kong MG, Ostrikov K. Atmospheric pressure plasmas: infection control and bacterial responses. *Int J Antimicrob Agents*. 2014;43(6):508-517. doi: 10.1016/J.IJANTIMICAG.2014.01.025

31. Aboubakr HA, Mor SK, Higgins L, et al. Cold argon-oxygen plasma species oxidize and disintegrate capsid protein of feline calicivirus. *PLoS One*. 2018;13(3):e0194618. doi: 10.1371/journal.pone.0194618

32. Aboubakr HA, Nauertz A, Luong NT, et al. In vitro antiviral activity of clove and ginger aqueous extracts against feline calicivirus, a surrogate for human norovirus. *J Food Prot*. 2016;79(6):1001-1012. doi: 10.4315/0362-028X.JFP-15-593

33. Xu D, Ning N, Xu Y, et al. Effect of cold atmospheric plasma treatment on the metabolites of human leukemia cells. *Cancer Cell Int*. 2019;19(1):1-12. doi: 10.1186/s12935-019-0856-4

34. Zimmermann JL, Dumler K, Shimizu T, et al. Effects of cold atmospheric plasmas on adenoviruses in solution. *J Phys D Appl Phys*. 2011;44(50):505201. doi: 10.1088/0022-3727/44/50/505201

35. Sakudo A, Toyokawa Y, Imanishi Y, Murakami T. Crucial roles of reactive chemical species in modification of respiratory syncytial virus by nitrogen gas plasma. *Mater Sci Eng C*. 2017;74:131-136. doi: 10.1016/j.msec.2017.02.007

36. Sakudo A, Misawa T, Shimizu N, Imanishi Y. N_2 gas plasma inactivates influenza virus mediated by oxidative stress. *Front Biosci (Elite Ed)*. 2014;6(1):69-79. doi: 10.2741/E692

37. Sakudo A, Toyokawa Y, Imanishi Y. Nitrogen gas plasma generated by a static induction thyristor as a pulsed power supply inactivates adenovirus. *PLoS One*. 2016;11(6):e0157922. doi: 10.1371/JOURNAL.PONE.0157922

38. Alkawareek MY, Algwari QT, Gorman SP, Graham WG, O'Connell D, Gilmore BF. Application of atmospheric pressure nonthermal plasma for the in vitro eradication of bacterial biofilms. *FEMS Immunol Med Microbiol*. 2012;65(2):381-384. doi: 10.1111/j.1574-695X.2012.00942.x

39. Haertel B, Woedtke T von, Weltmann KD, Lindequist U. Non-thermal atmospheric-pressure plasma possible application in wound healing. *Biomol Ther*. 2014;22(6):477-490. doi: 10.4062/biomolther.2014.105

40. Guo L, Xu R, Gou L, et al. Mechanism of virus inactivation by cold atmospheric-pressure plasma and plasma-activated water. *Appl Environ Microbiol*. 2018;84(17):1-10. doi: 10.1128/AEM.00726-18

41. Dolezalova E, Lukes P. Membrane damage and active but nonculturable state in liquid cultures of *Escherichia coli* treated with an atmospheric pressure plasma jet. *Bioelectrochemistry*. 2015;103:7-14. doi: 10.1016/J.BIOELECHEM.2014.08.018

42. Haas M, Fürhacker P, Hodek J, et al. Detection of viable SARS-CoV-2 on the hands of hospitalized children with COVID-19. *Clin Microbiol Infect*. 2023;29(9):1211-1213.

doi: 10.1016/J.CMI.2023.06.012

43. Nogueira F, Obrova K, Haas M, et al. Intestinal shedding of SARS-CoV-2 in children: no evidence for infectious potential. *Microorganisms*. 2023;11(1):33. doi: 10.3390/microorganisms11010033

44. Lion T. Adenovirus persistence, reactivation, and clinical management. *FEBS Lett*. 2019;593(24):3571-3582. doi: 10.1002/1873-3468.13576

45. Lion T, Wold W. Adenoviruses. In: Knipe D, Howley P, eds. *Chapter in Fields Virology*, 7th ed. Wolters Kluver Health / Lippincott, Williams Wilkins 2022, 129-171. https://www.livres-medicaux.com/infectiologie-virologie-bacteriologie/23602-fields-virology-dna-viruses-vol-2-7th-ed.html. Accessed July 25, 2023.

46. Leung NHL. Transmissibility and transmission of respiratory viruses. *Nat Rev Microbiol*. 2021;19(8):528-545. doi: 10.1038/s41579-021-00535-6

47. Kirtipal N, Bharadwaj S, Gu S. From SARS to SARS-CoV-2, insights on structure, pathogenicity and immunity aspects of pandemic human coronaviruses. *Infect Genet Evol*. 2020;85(January):15. doi: 10.1016/j.meegid.2020.104502

48. Kumar V. Influenza in children. *Indian J Pediatr*. 2017;84(2):139-143. doi: 10.1007/s12098-016-2232-x

49. Lion T. Adenovirus infections in immunocompetent and immunocompromised patients. *Clin Microbiol Rev*. 2014;27(3):441-462. doi: 10.1128/CMR.00116-13

50. Piotrowska Z, Vázquez M, Shapiro ED, et al. Rhinoviruses are a major cause of wheezing and hospitalization in children less than 2 years of age. *Pediatr Infect Dis J*. 2009;28(1):25-29. doi: 10.1097/INF.0b013e3181861da0

51. Fazeli N, Momtaz H. Virulence gene profiles of multidrug-resistant *Pseudomonas aeruginosa* isolated from Iranian hospital infections. *Iran Red Crescent Med J*. 2014;16(10). doi: 10.5812/ircmj.15722

52. Ranjan Prasad R, Shree V, Kumar R, Kala K, Kumar P. Prevalence and antibiotic sensitivity of *Pseudomonas aeruginosa* isolated from CSOM in NMCH, Patna, India. *Int J Curr Microbiol Appl Sci*. 2017;6(6):2912-2916. doi: 10.20546/ijcmas.2017.606.345

53. Khun J, Machková A, Kašparová P, et al. Non-thermal plasma sources based on cometary and point-to-ring discharges. *Molecules*. 2022;27(1):238. doi: 10.3390/molecules27010238

54. Kašparová P, Vaňková E, Paldrychová M, et al. Nonthermal plasma causes *Pseudomonas aeruginosa* biofilm release to planktonic form and inhibits production of Las-B elastase, protease and pyocyanin. *Front Cell Infect Microbiol*. 2022;12(September):1-16. doi: 10.3389/fcimb.2022.993029

55. Ngaosuwankul N, Noisumdaeng P, Komolsiri P, et al. Research influenza A viral loads in respiratory samples collected from patients infected with pandemic H1N1, seasonal H1N1 and H3N2 viruses. *Virol J*. 2010;7(1):1-7. doi: 10.1186/1743-422X-7-75/TABLES/4

56. Machala Z, Tarabová B, Sersenová D, Janda M, Hensel K. Chemical and antibacterial effects of plasma activated water: correlation with gaseous and aqueous reactive oxygen and nitrogen species, plasma sources and air flow conditions. *J Phys D Appl Phys*. 2019;52(3):034002. doi: 10.1088/1361-6463/aae807

57. Kučerová K, Machala Z, Hensel K. Transient spark discharge generated in various N_2/O_2 gas mixtures: reactive species in the gas and water and their antibacterial effects. *Plasma Chem Plasma Process*. 2020;40(3):749-773. doi: 10.1007/s11090-020-10082-2

58. Lukes P, Dolezalova E, Sisrova I, Clupek M. Aqueous-phase chemistry and bactericidal effects from an air discharge plasma in contact with water: evidence for the formation of peroxynitrite through a pseudo-second-order postdischarge reaction of H_2O_2 and HNO_2. *Plasma Sources Sci Technol*. 2014;23(1):015019. doi: 10.1088/0963-0252/23/1/015019

59. Wang Z, Liu L, Liu D, et al. Combination of NO_x mode and O_3 mode air discharges for water activation to produce a potent disinfectant. *Plasma Sources Sci Technol*. 2022;31(5):05LT01. doi: 10.1088/1361-6595/ac60c0

60. Dasan BG, Onal-Ulusoy B, Pawlat J, Diatczyk J, Sen Y, Mutlu M. A New and Simple Approach for Decontamination of Food Contact Surfaces with Gliding Arc Discharge Atmospheric Non-Thermal Plasma. *Food Bioprocess Technol*. 2017;10(4):650-661. doi: 10.1007/S11947-016-1847-2

61. Belgacem Z Ben, Carre G, Charpentier E, et al. Innovative nonthermal plasma disinfection process inside sealed bags: Assessment of bactericidal and sporicidal effectiveness in regard to current sterilization norms. *PLoS One*. 2017;12(6):e0180183. doi: 10.1371/JOURNAL.PONE.0180183

62. Lunov O, Zablotskii V, Churpita O, et al. The interplay between biological and physical scenarios of bacterial death induced by nonthermal plasma. *Biomaterials*. 2016; 82:71-83. doi: 10.1016/J.BIOMATERIALS.2015.12.027

63. Scholtz V, Pazlarova J, Souskova H, Khun J, Julak J. Nonthermal plasma---a tool for decontamination and disinfection. *Biotechnol Adv*. 2015;33(6 Pt 2):1108-1119. doi: 10.1016/J.BIOTECHADV.2015.01.002

64. Alkawareek MY, Gorman SP, Graham WG, Gilmore BF. Potential cellular targets and antibacterial efficacy of atmospheric pressure nonthermal plasma. *Int J Antimicrob Agents*. 2014;43(2):154-160. doi: 10.1016/J.IJANTIMICAG.2013.08.022

65. Jablonowski H, Hänsch MAC, Dünnbier M, et al. Plasma jet's shielding gas impact on bacterial inactivation. *Biointerphases*. 2015;10(2):029506. doi: 10.1116/1.4916533

66. Machala Z, Tarabova B, Hensel K, Spetlikova E, Sikurova L, Lukes P. Formation of ROS and RNS in water electro-sprayed through transient spark discharge in air and their bactericidal effects. *Plasma Process Polym*. 2013;10(7):649-659. doi: 10.1002/PPAP.201200113

67. Oehmigen K, Hähnel M, Brandenburg R, Wilke C, Weltmann KD, Von Woedtke T. The role of acidification for antimicrobial activity of atmospheric pressure plasma in liquids. *Plasma Process Polym*. 2010;7(3-4):250-257. doi: 10.1002/PPAP.200900077

68. Liu Z, Xu D, Liu D, et al. Production of simplex RNS and ROS by nanosecond pulse N_2/O_2 plasma jets with homogeneous shielding gas for inducing myeloma cell apoptosis. *J Phys D Appl Phys*. 2017;50(19):195204. doi: 10.1088/1361-6463/aa66f0

69. Ke Z, Thopan P, Fridman G, et al. Effect of N_2/O_2 composition on inactivation efficiency of *Escherichia coli* by discharge plasma at the gas-solution interface. *Clin Plasma Med*. 2017;7-8:1-8. doi: 10.1016/j.cpme.2017.05.001

70. Thurston-Enriquez JA, Haas CN, Jacangelo J, Riley K, Gerba CP. Inactivation of Feline Calicivirus and Adenovirus Type 40 by UV Radiation. *Appl Environ Microbiol*. 2003;69(1):577-582. doi: 10.1128/AEM.69.1.577-582.2003

71. Von Woedtke T, Laroussi M, Gherardi M. Foundations of plasmas for medical applications. *Plasma Sources Sci Technol*. 2022;31(5):054002. doi: 10.1088/1361-6595/AC604F

72. Bisag A, Isabelli P, Laurita R, et al. Cold atmospheric plasma inactivation of aerosolized microdroplets containing bacteria and purified SARS-CoV-2 RNA to contrast airborne indoor transmission. *Plasma Process Polym*. 2020;17(10):1-8. doi: 10.1002/ppap.202000154

73. Kobza J, Geremek M, Dul L. Ozone concentration levels in urban environments—upper Silesia region case study. *Int J Environ Res Public Heal 2021, Vol 18, Page 1473*. 2021;18(4):1473. doi: 10.3390/IJERPH18041473

74. Wolfgruber S, Loibner M, Puff M, Melischnig A, Zatloukal K. SARS-CoV-2 neutralizing activity of ozone on porous and nonporous materials. *N Biotechnol*. 2022;66:36-45. doi: 10.1016/j.nbt.2021.10.001

75. Mileto D, Mancon A, Staurenghi F, et al. Inactivation of SARS-CoV-2 in the liquid phase: are aqueous hydrogen peroxide and sodium percarbonate efficient decontamination agents? *ACS Chem Heal Saf*. 2021;28(4):260-267. doi: 10.1021/acs.chas.0c00095

76. Mentel R, Schirrmacher R, Kewitsch A. Inactivation of viruses with hydrogen dioxide. *Vopr Virusol*. 1977;22(6):731-733. Accessed March 30, 2023. http://www.ncbi.nlm.nih.gov/pubmed/203115

77. Amanna IJ, Raué HP, Slifka MK. Development of a new hydrogen peroxide–based vaccine platform. *Nat Med 2012 186*. 2012;18(6):974-979. doi: 10.1038/nm.2763

78. Termini J. Hydroperoxide-induced DNA damage and mutations. *Mutat Res Mol Mech Mutagen*. 2000;450(1-2):107-124. doi: 10.1016/S0027-5107(00)00019-1

79. Wang H, Zhao T, Yang S, Zou L, Wang X, Zhang Y. Reactive force field-based molecular dynamics simulation of the interaction between plasma reactive oxygen species and the receptor-binding domain of the spike protein in the capsid protein of SARS-CoV-2. *J Phys D Appl Phys*. 2021;55(9):095401. doi: 10.1088/1361-6463/AC360E

80. Sahun M, Privat-Maldonado A, Lin A, et al. Inactivation of SARS-CoV-2 and other enveloped and non-enveloped viruses with non-thermal plasma for hospital disinfection. *ACS Sustain Chem Eng*. 2023;11(13):5206-5215. doi: 10.1021/acssuschemeng.2c07622